Successive electric polarization transitions induced by high magnetic field in the single-crystal antiferromagnet $Co_2Mo_3O_8$

Y. S. Tang,[1] G. Z. Zhou,[1] L. Lin,[2,*] R. Chen,[3] J. F. Wang,[3] C. L. Lu,[3] L. Huang,[1] J. H. Zhang,[1] Z. B. Yan,[1] X. M. Lu,[1] X. K. Huang,[4] X. P. Jiang,[4] and J.-M. Liu[1]

[1]*Laboratory of Solid State Microstructures and Innovation Center of Advanced Microstructures, Nanjing University, Nanjing 210093, China*

[2]*Department of Applied Physics, College of Science, Nanjing Forestry University, Nanjing 210037, China*

[3]*Wuhan National High Magnetic Field Center and School of Physics, Huazhong University of Science and Technology, Wuhan 430074, China*

[4]*School of Materials Science and Engineering, Jingdezhen Ceramic Institute, Jingdezhen 333403, China*

(Received 19 October 2021; revised 14 January 2022; accepted 3 February 2022; published 22 February 2022)

The polar antiferromagnet $Co_2Mo_3O_8$ was recently reported as a new multiferroic material exhibiting remarkable second-order magnetoelectric (ME) coupling effect while no other metamagnetic transitions occurred at low magnetic field. Herein, we have investigated the ME phenomena under high magnetic field (up to 60 T) in $Co_2Mo_3O_8$ single crystals and observed unique ME response associated with the changes in the hidden magnetic moment on the honeycomb lattice. Two spin-flop transitions are unambiguously defined at $H_{c1} \sim 27$ T and $H_{c2} \sim 31$ T under H along the c axis at 1.7 K, accompanied by two successive colossal changes of electric polarization. The results on the anisotropy of magnetoelectricity as well as the angular-dependent polarization are well consistent with the ME tensor prediction, providing a better approach to understand the evolution of magnetic structures under high magnetic field. Therefore, the hidden magnetic transitions and distinctive magnetoelectricity provide a unique platform on which the ME coupling mechanism in the presence of rich magnetic phase transitions can be explored in this 238 family.

DOI: 10.1103/PhysRevB.105.064108

I. INTRODUCTION

The response of electric polarization (P) to a magnetic field (H) or magnetization (M) to an electric field (E), namely magnetoelectric (ME) effect, has attracted great attention due to the intriguing physics underpinning this effect and their exciting potential for application and novel functional devices [1–3]. Among them, significant efforts have been devoted to the search for new multiferroic materials with combining and control of these simultaneous ferroelectric and magnetic orderings. They are usually classified into two types according to their different microscopic mechanisms of electric polarization (P) [4]. In type-II multiferroics, the ferroelectricity is induced by a particular type of magnetic ordering via the spin-orbit coupling, whereas the spin reorientation is very flexible to the magnetic field and ME coupling is intrinsic and strong. However, as the specific magnetic orders originate from the competition between nearest-neighbor and further-neighbor magnetic exchange of comparable strength, the similar strength is usually found in a small value with strong magnetic frustration; thus, the spin-driven ferroelectricity usually establishes in a relative low temperature (T) [5–9]. On the contrary, robust ferroelectric order can develop at high temperatures in the type-I multiferroics, while a separate magnetic sublattice orders at low temperature and couples weakly to P due to their independent origins [10–13].

Based on the dilemma of multiferroics discussed above, seeking new ME materials with strong coupling at high temperature is challenging, requiring development of a new foothold in the emerging ME phenomena. The linear magnetoelectricity, which exhibits magnetic field-driven P at relatively higher T than typical type-II multiferroics, has been attracting a great deal of attention [14–16]. A common feature is that they usually offer nonpolar magnetic point group with ferroelectricity inactive (FE-inactive) state as shown in Fig. 1(a), while a ferroelectricity active (FE-active) state can be induced by external magnetic stimuli. The magnetic structure changes from the nonpolar M_1 state to polar M_2 state, which simultaneously breaks the space inversion and time-reversal symmetry, giving rise to nontrivial ME effects. Obviously, in this case, the FE-active state is severely restricted by over ~meV of the magnetic energy barrier between the M_1 state and M_2 state, hindering the way to uncover the coupling between ferroic orderings [17,18]. An alternative way is to seek materials both belonging to the polar crystallographic symmetry groups and polar magnetic point groups. Consequently, such polar magnet should exhibit nontrivial ME effects below magnetic ordering temperature. Moreover, it is noted that in some cases the macroscopic magnetic moment is nearly buried in the antiferromagnetic (AFM) ground state. Upon applying magnetic field, the hidden magnetic transitions, e.g., spin-flop, magnetization plateau, or ferromagnetic transition can be easily uncovered [19–21]. These hidden magnetic transitions and distinctive magnetoelectricity provide a unique platform on which the ME coupling mechanism in the presence of rich magnetic phase transitions can be explored.

*llin@njfu.edu.cn

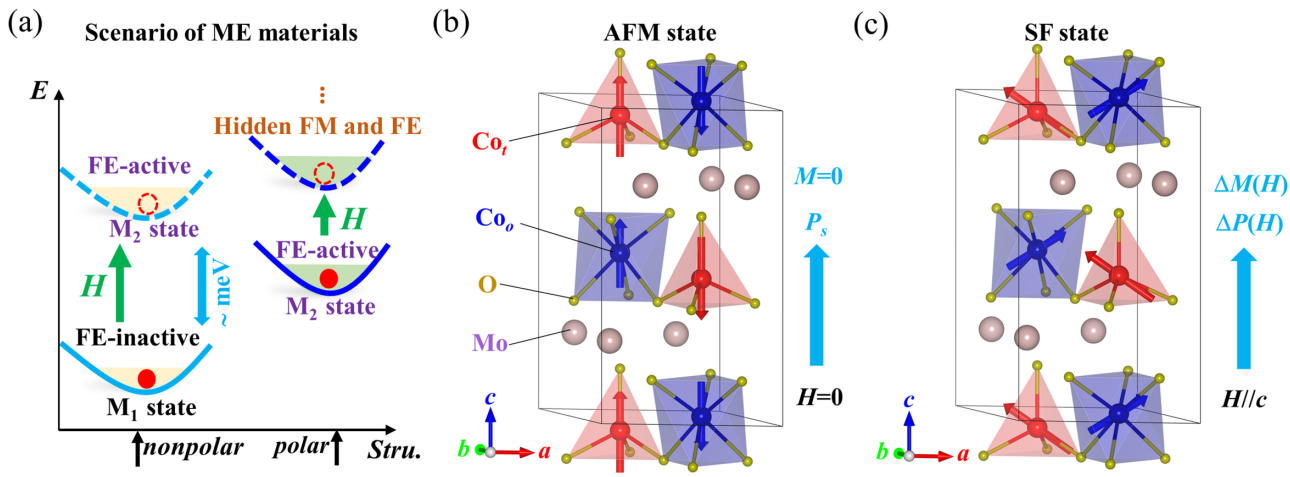

FIG. 1. (a) A proposed scenario of realizing ME coupling effect. The M_1 and M_2 states represent the ferroelectricity-inactive (FE-inactive) and ferroelectricity-active (FE-active) states, respectively. The dashed lines and hollow red spheres represent the hidden states induced by H. (b) Crystal structure and AFM magnetic structure of $Co_2Mo_3O_8$. (c) Possible hidden magnetic structure magnetically induced EF-active states. The $\Delta P(H)$ and $\Delta M(H)$ represent the H-induced polarization and magnetization, respectively.

Most recently, the magnetoelectricity in the family of $A_2Mo_3O_8$ (A = Fe, Mn, Co, and Ni) has drawn strong attention [22–25], like the honored $Fe_2Mo_3O_8$, which possess the hidden ferrimagnetism and FE-active states under H. Here, it is noted that the polar magnetic point group of $Co_2Mo_3O_8$ characterized as $6'mm'$ in the AFM ground state, as shown in Fig. 1(b), is the same as that in $Fe_2Mo_3O_8$ with the polar axis pointing to the c direction. Nonetheless, the ME coupling effect in $Co_2Mo_3O_8$ contrasts to any other members, in which only the second-order ME effect in terms of magnetic field dependence of ferroelectric polarization response has been observed in $Co_2Mo_3O_8$. Moreover, $Co_2Mo_3O_8$ shows robust AFM behavior with no other magnetic transitions up to 9 T, deserving high magnetic field strategy to unveil the hidden magnetism and underlying magnetoelectricity. The previous neutron scattering indicates that the magnetic moments on the tetrahedral and octahedral sites are highly correlated with different moment ($M_t = 3.44\,\mu_B/\mathrm{Co}_t$, $M_o = 3.35\,\mu_B/\mathrm{Co}_o$) [24]. Similar to the case of $Fe_2Mo_3O_8$, $Co_2Mo_3O_8$ may display successive metamagnetic transitions under high H, e.g., spin flop (SF) or ferrimagnetic transition [22]. As illustrated in the SF state shown in Fig. 1(c), a combination of net magnetization ΔM and electric polarization ΔP should be acquired in the high-H region.

In this work, we present two successive phase transitions in $Co_2Mo_3O_8$ single crystals by high magnetic field study up to 60 T. Unlike the ferrimagnetism in $Fe_2Mo_3O_8$, two spin-flop transitions are unambiguously defined under H along the c axis, accompanied by two successive electric polarization transitions, indicating intrinsic ME coupling effect. We corroborate our experimental results with ME tensor analysis in the ground state, thereby interpreting the magnetic structure changes and origins of the ME coupling effect. Our results imply that $Co_2Mo_3O_8$ with spin-3/2 embodying two distinctive SF and FE-active states is different from other linear ME materials in this 238 system.

II. EXPERIMENT DETAILS

$Co_2Mo_3O_8$ single crystals were grown by the chemical vapor transport technique as described earlier [26]. The characterization of the sample quality can be found in the previous work [24]. The T dependence of magnetic susceptibility (χ) were measured using the Quantum Design Superconducting Quantum Interference Device (SQUID) magnetometer (MPMS, Quantum Design) from 5 to 300 K under the zero field-cooling (ZFC) and field-cooling (FC) modes with cooling magnetic field $H = 0.2$ T along $H//c$ and $H\perp c$, respectively. For polarization measurement, two single crystals were cut into a slice shape with the surface parallel and normal to the c direction. Silver paste was painted on the surfaces of the specimens as the electrodes. The magnetoelectric current and field-induced electric polarization were obtained by conventional pyroelectric measurement. Similar to the previous report on $Fe_2Mo_3O_8$ [22], our grown crystals are also monodomains, as the T-dependent pyroelectric current remains unchanged no matter whether poling electric field is applied, reversed, or not, implying that robust polar domains were already formed in the raw crystals. In detail, the sample was cooled from 60 K to target T without any E or H. The short-circuited procedure for sufficient time was performed before each measurement to avoid the influence of the injected charge. When the background of electrical current was less than 0.1 pA, the magnetoelectric current $\Delta I_c(H)$ under $H//c$, $H\perp c$ and changing the direction of H away from the c axis 45 ° geometries were measured using Keithley 6514 programmable electrometer at ramping magnetic field from -8 to 8 T at a rate of 100 Oe/s. The electric polarization ΔP was obtained by integrating the magnetocurrent with the time.

For the high magnetic field parts, the $M(H)$ of in-plane and out-of-plane were measured at selected temperatures in the pulse-field modes, using a coaxial pickup coil and calibrated by a comparison with the low-field data measured by SQUID. Simultaneously, the H dependent high field-induced polariza-

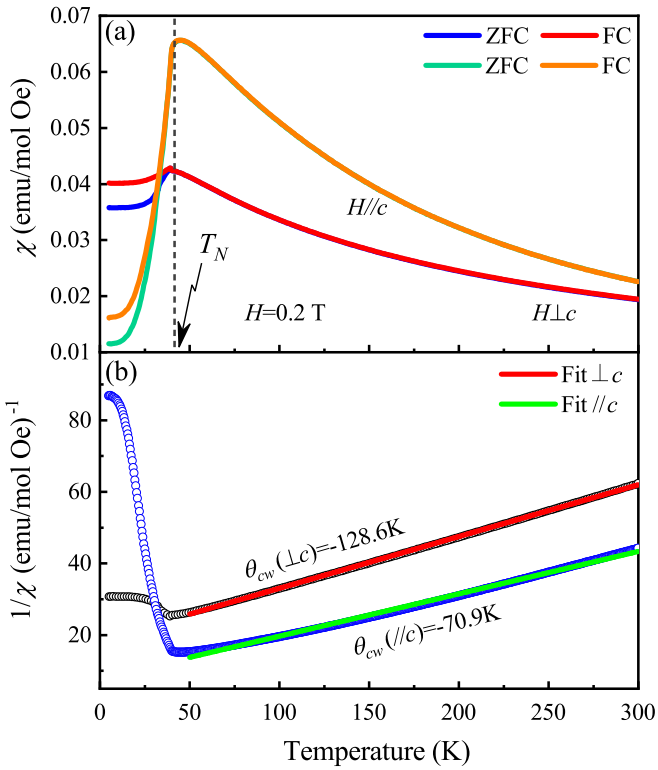

FIG. 2. (a) The measured magnetic susceptibility $\chi(T)$ as a function of T, and (b) the Curie-Weiss fitting χ^{-1} measured along c axis and normal to c axis, respectively.

tion $\Delta P_c(H)$ was measured in the $H//c$ modes at different T. All the high-field M and ΔP were measured using 10.5-ms short-pulse magnet in the Wuhan National High Magnetic Field Center.

III. RESULTS AND DISCUSSION

A. Magnetic susceptibility and hidden spin-flop states

Figure 2(a) shows the T dependence of $\chi(T)$ in the ZFC and FC modes with measuring field of 0.2 T in the geometry aligned parallel to the c axis [$\chi_c(T)$] and normal to the c axis [$\chi_{ab}(T)$], respectively. The $\chi(T)$ exhibit a cusp at Néel temperature (T_N) ~ 40.5 K in both $\chi_c(T)$ and $\chi_{ab}(T)$, suggesting the formation of AFM ordering. It is noted that our previous polycrystalline sample shows a small peak at T_N [24], while it is absent in single crystal, implying less amount of ferromagnetic impurities. In fact, the magnetic susceptibility is very consistent with previously reported data in their single crystals [26], demonstrating high quality of our crystals. The large difference between the magnetic susceptibility curves along these two directions implies that the easy axis points to the c direction. We have fitted the linear part of inverse magnetic susceptibility $1/\chi(T)$ between 50 and 300 K to the Curie-Weiss law, as shown in Fig. 2(b):

$$\chi(T) = \chi_0 + \frac{C}{T + \theta_{cw}}, \tag{1}$$

where χ_0 accounts for temperature-independent contribution. The second term in Eq. (1) is the Curie-Weiss (CW) law with the CW temperature θ_{cw} and Curie constant C. One can obtain the Curie-Weiss temperature as $\theta_{cw}(//c) \sim -70.9$ K and $\theta_{cw}(\perp c) \sim -128.6$ K, and the effective magnetic moment $\mu_{\text{eff}}(//c) = 4.127\,\mu_B$/Co and $\mu_{\text{eff}}(\perp c) = 3.734\,\mu_B$/Co, respectively. The detailed values fitted from the Curie-Weiss law are listed in Table I. It is noted that the measured effective moment along the c axis is intermediate between the spin-only value $p_S = 3.87\,\mu_B$/Co and the total spin value $p_J = 6.63\,\mu_B$/Co, indicating incomplete quenching of the orbital moment. This result is very similar to the previously reported spin-orbit coupling materials, commonly consisting in the Co^{2+} ions compounds [27].

Our previous report shows that the magnetization along the c axis [$M_c(H)$] and perpendicular to the c axis [$M_{ab}(H)$] exhibits perfect linear responses to H, uncovering robust AFM behavior in the low-H region ($H < 9$ T) [24]. In order to reveal the potential magnetic transitions as well as the underneath ME coupling phenomenon and mechanism, we used pulsed high magnetic field facility to measure the magnetization and electric polarization. Figure 3(a) shows the magnetic field dependence of the magnetization $M_c(H)$ up to 40 T at selected temperatures. Two successive metamagnetic transitions occurring at critical fields H_{c1} and H_{c2} are unambiguously defined. With increasing T, the low critical field H_{c1} stays almost unchanged, while H_{c2} shifts a little bit to the low field, and finally both of them vanish near T_N. When H is further increased to 60 T, there are no other transitions except the two successive spin-flop (named as SF1 and SF2, respectively) transitions with $H//c$ as shown in Fig. 3(b). However, the magnetization has not saturated yet considering the theoretically spin-only saturated magnetic moment $M_{\text{sat}} \sim 7.74\,\mu_B$/formula. Here, the two spin-flop transitions can be more clearly identified in the dM_c/dH curve in Fig. 3(c), While on the other side, it is evident that there is still absence of any metamagnetic transitions in the ab plane, as shown in Fig. 3(b), suggesting robust AFM interaction under the case of $H \perp c$.

Now one is allowed to give a tentative discussion on the magnetic structure by combing the data on magnetization and previous reports on this 238 family. The neutron scattering has confirmed the magnetic point group $6'mm'$ to describe the c axis collinear antiferromagnetic ground state, as shown in Fig. 3(d), same to that in $Fe_2Mo_3O_8$ [19,22]. Hence, we believe that the two successive spin-flop transitions with $H//c$ are also caused by the Co^{2+} ions at tetrahedral and octahedral sites with different moments (named as Co_t and Co_o), e.g., 3.44(1) μ_B for Co_t and 3.35(1) μ_B for Co_o site [24]. A collinear ferrimagnetic state was observed in $Fe_2Mo_3O_8$ under $H//c$ and $Mn_2Mo_3O_8$ with the local magnetic moments are along the c axis all the time, corresponding to the magnetic point group $6\,m'm'$ [19]. Nevertheless, the spin-flop transitions in $Co_2Mo_3O_8$, including the case of $Mn_2Mo_3O_8$ under $H//c$, are very different from the ferrimagnetic states of $Fe_2Mo_3O_8$ with a spin order single along the c axis. When the system enters into SF1 phase, all the Co^{2+} spins rotate towards to the direction perpendicular to the c axis, noting that Co_t carrying large moment tends to align along the direction of the magnetic field, while Co_o spin points to the opposite direction due to the stronger AFM interaction, as shown in Fig. 3(e). For the field $H > H_{c2}$, the field is large enough to overcome the AFM

TABLE I. The AFM ordering temperature, Curie-Weiss temperature, and effective moment for $Co_2Mo_3O_8$ single crystal in the geometry aligned parallel to c axis and normal to c axis.

$Co_2Mo_3O_8$	T_N(K)	θ_{cw}(K)	C	μ_{eff} (μ_B)	$g\sqrt{S(S+1)}$	$g_J\sqrt{J(J+1)}$
c axis	40.5	−70.9	8.446	4.127	3.873	6.633
ab plane	40.5	−128.6	6.913	3.734	3.873	6.633

exchange interaction between the nearest-neighbor Co^{2+}, so that all the Co^{2+} spins tend to have net magnetization along the field, as shown in Fig. 3(f).

Of course, it is very difficult for us to speculate the magnetic point groups in these two hidden spin-flop states, which present noncollinear spin structure. The neutron scattering experiment under magnetic field or theoretical calculations are highly required to resolve the exact magnetic structures, which are actually beyond the scope of our work. It is noted that similar hidden states can be found in other ME materials, such as $Ni_2Mo_3O_8$ [21], $Co_2V_2O_7$ [28], $Ni_3V_2O_8$ [29], and $PbCu_3TeO_7$ [30]. Subsequently, we turn to the main issue and discuss the ME effect in the high-H region.

B. Hidden magnetoelectricity

To unveil the hidden magnetoelectricity under the high-H region in $Co_2Mo_3O_8$, we present the c-axis magnetoelectric current ΔI_c and electric polarization ΔP_c as a function of magnetic field applied along the c axis at selected T as shown in Figs. 4(a) and 4(b). At low temperature, e.g., $T = 5$ K amplified in the inset of Fig. 4(a), a small broad bump appears at $H_{c1} \sim 27$ T, accompanied by a sharp peak at $H_{c2} \sim 31$ T, concomitant with the onset of two successive SF transitions in $M_c(H)$ as shown in Fig. 4(c). The most striking feature of the high-field transition is the two successive colossal changes of polarization (ΔP_c) at critical fields as well as the emergence of linear ME coupling effect, which is absent in low field. It

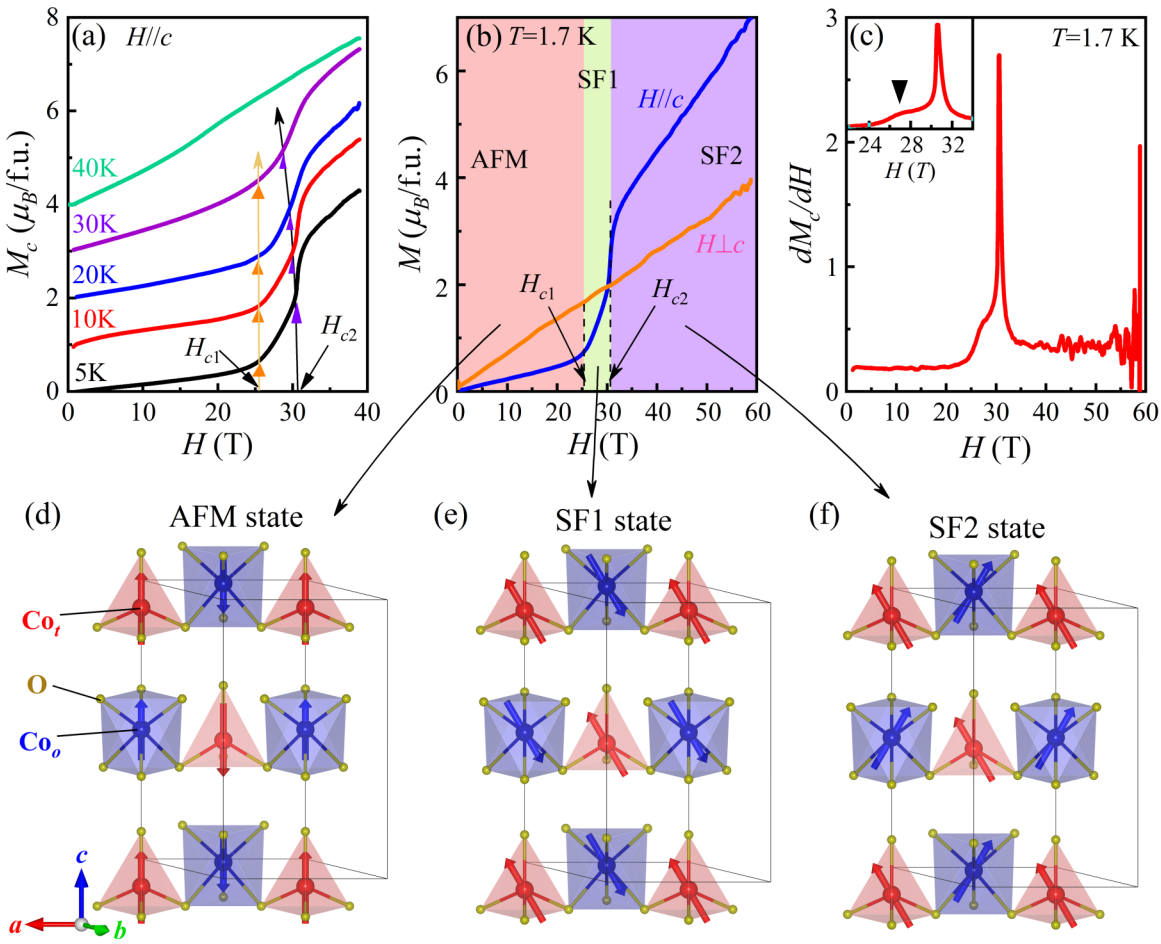

FIG. 3. The H dependence of the magnetization. (a) $M_c(H)$ with increasing H up to 40 T under selected T. (b) $M_c(H)$ and $M_{ab}(H)$ with increasing H up to 60 T at $T = 1.7$ K, respectively. (c) The derivative of the magnetization dM_c/dH with increasing H up to 60 T at $T = 1.7$ K, respectively. (d)–(f) The schematic magnetic structure in the AFM, SF1, and SF2 states. The red and blue arrows represent the magnetic moment on the tetrahedron and octahedron sites, respectively.

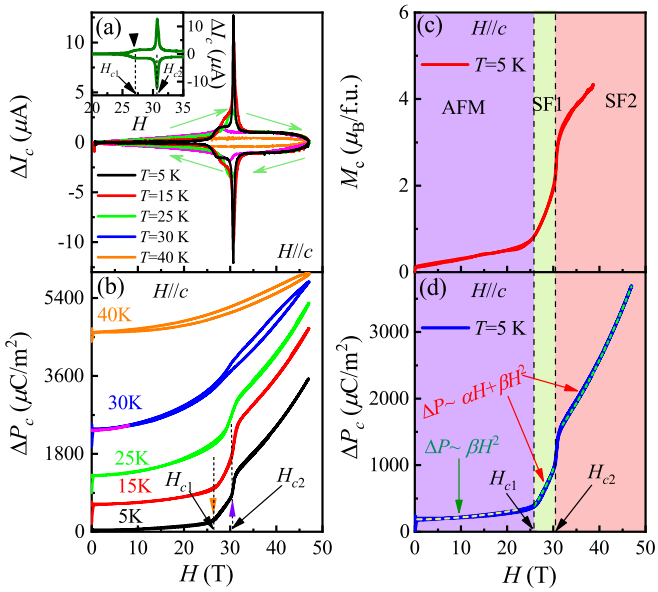

FIG. 4. (a) The magnetocurrent (ΔI_c) and (b) polarization (ΔP_c) with respect to the magnetic field for fields $H//c$ up to 48 T measured at selected T, respectively. Note that the curves are shown with an offset and that the absolute value of the offset should be ignored. (c) The $M_c(H)$ and (d) and the ΔP_c (H) with $H//c$ at $T = 5$ K. The dashed lines are the fits to the ΔP_c-H curve with the different functions of $\Delta P_c \sim \beta H^2$ and $\Delta P_c \sim \alpha H + \beta H^2$, where α and β are constants.

is noted that a jump of polarization near zero magnetic field is caused by the high-field instrument, and is irrelevant to the samples. For a better illustration, the H-dependent ΔP_c measured at different temperatures are vertically shifted to show the features more clearly, and the absolute value of the offset should be ignored. In addition, the behavior of the critical fields in which the polarization transitions are consistent with that in the magnetization, indicating intriguing ME effect.

According to the $\Delta P_c(H)$ data in Fig. 4(c), one can see that the two hidden spin-flop phases are obviously characterized by inducing linear ME effect, while below H_{c1}, the H-induced ΔP_c is well identified as the quadratic ME effect. Generally, ΔP_c can be given as a function of H extended to the second order as follows:

$$\Delta P = P_c + P_s + \alpha H + \beta H^2, \tag{2}$$

where P_c and P_s are the crystallographic and spin-induced spontaneous polarization, which are finite even under zero field. The tensors α and β correspond to the first-order and second-order ME coefficients, respectively [23]. Here, we exemplify one of the fits as the dashed lines at $T = 5$ K as shown in Fig. 4(d). It can be seen that ΔP_c is quadratic to H for $H > H_{c1}$, and the second-order ME coefficient β_{ccc} well reproduces the result of Ref. [24]. In addition, for $H > H_{c1}$ region, the $\Delta P_c(H)$ data show good fitting by introducing the linear relation part. We obtain the first-order ME coefficients $\alpha_{cc} = 12$ and 28 ps/m for the SF1 and SF2 states, respectively. Here, the large value in SF2 state corresponds to both the Co_t and Co_o spins tending to magnetic field larger than that in SF1 state, in which Co_t carrying large moment tends to align along the direction of the magnetic field, while Co_o spin points to the opposite direction due to the stronger AFM interaction. It is noted that both of the spin-flop transitions allow second-order term, but show very weak effect. By fitting the data of $\Delta P_c(H)$ in Figs. 4(b) and 4(d), we can obtain the second-order ME coefficient in the spin-flop states as $\beta_{ccc} = 1.14\times10^{-22}$ s/A and 5.3×10^{-22} s/A for the SF1 and SF2 states, respectively, much smaller than that in the antiferromagnetic state with $\beta_{ccc} = 29.59\times10^{-19}$ s/A [24]. Combining the results of magnetism and electric polarization, it is seen that $Co_2Mo_3O_8$ exhibits two hidden spin-flop and FE-active states under the high H, thus providing insights on design materials with strong magnetoelectric coupling.

C. Discussion

As mentioned above, our results reveal two successive magnetic field-induced electric polarization switching. Here, we focus our attention on the ME tensor analysis to help us better understand the transformation of magnetic structure and coherent ME effect. The Cartesian coordinates, $\boldsymbol{x} = \boldsymbol{a}$, $\boldsymbol{y} = \boldsymbol{a} + 2\boldsymbol{b}, \boldsymbol{z} = \boldsymbol{c}$, in which $\boldsymbol{a}$, $\boldsymbol{b}$, and $\boldsymbol{c}$ are the crystallographic axes for this hexagonal crystal structure and magnetic structure are defined [31]. Below the SF1 state, the magnetic point group is $6'mm'$, which is polar and only allows nonlinear ME effect. The ME tensor β_{ijk} for this AFM state is given as [32]

$$\begin{pmatrix} 0 & 0 & \beta_{xxz} \\ 0 & 0 & 0 \\ \beta_{xxz} & 0 & 0 \end{pmatrix} \begin{pmatrix} 0 & 0 & 0 \\ 0 & 0 & \beta_{yyz} \\ 0 & \beta_{yyz} & 0 \end{pmatrix} \begin{pmatrix} \beta_{zxx} & 0 & 0 \\ 0 & \beta_{zyy} & 0 \\ 0 & 0 & \beta_{zzz} \end{pmatrix}. \tag{3}$$

Accordingly, the H-induced polarization ΔP_z can be written as

$$\Delta P_z(H) = \beta_{zxx} H_x H_x + \beta_{zyy} H_y H_y + \beta_{zzz} H_z H_z, \tag{4}$$

where the $\beta_{zxx} = \beta_{zyy}$, $\beta_{xxz} = \beta_{yyz}$ are second-order ME coefficients. We can obtain $\Delta P_c(H) = \beta_{ccc} {H_c}^2$ with magnetic field applied along the c axis, consistent with our experimental results as shown in Fig. 4(d). In order to further explore the anisotropy of ME tensor, $\Delta P_z(H)$ was measured by applying magnetic field normal to the z direction in AFM state. Figure 5(a) shows the polarization ΔP_z as a function of H applied perpendicular to the z axis at several temperatures. The quadratic relation data are well fitted by $\Delta P_z(H) \sim \beta_{zxx} {H_x}^2 + \beta_{zyy} {H_y}^2$ $(\beta_{zxx} = \beta_{zyy})$, consistent with the fact the magnetic point group for the AFM $(6'mm')$ state allows the nonzero second-order ME coefficient β_{zxx}.

Similarly, the in-plane component $\Delta P_{xy}(H)$ can be expressed as $\Delta P_{xy}(H) = 2\beta_{xxz} H_{xy} H_z$, where $H_{xy} = H\cos\theta$, $H_z = H\sin\theta$, and θ is the angle between the H and the z axis as shown in the schematic diagram in Fig. 5(c). Here, in principle, we present the calculated results of field-angle dependence of ΔP_{xy}. It can be clearly seen the induced electric polarization ΔP_{xy} changes its direction by an angle 2θ upon rotating the magnetic field by angle θ, consistent with that $\Delta P_{xy} = \beta_{xxz} H^2 \sin 2\theta$ is proportional to $\sin 2\theta$. To check this relation, Fig. 5(b) displays the case of $\Delta P_{xy}(H)$ under $\theta = 45^\circ$, and the results of is well fitted by the $\beta_{xxz} H^2$. In general, the ME coupling effect can be induced by external magnetic stimuli, which are large enough to overcome the magnetic

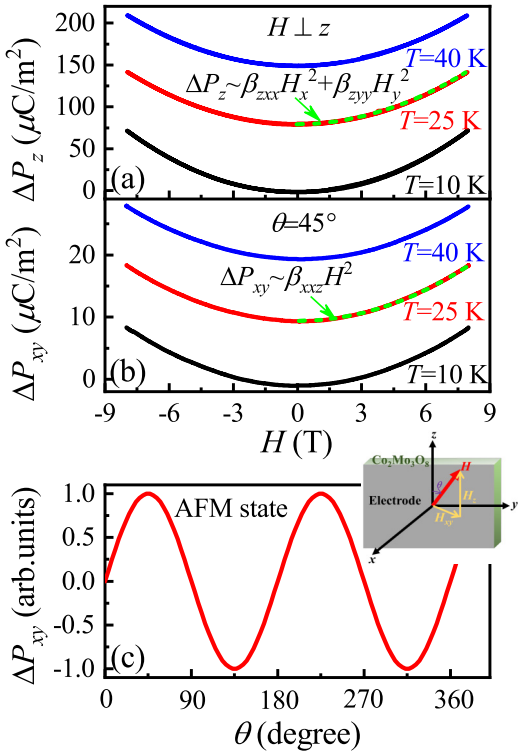

FIG. 5. (a) The H dependence of ΔP_z under $H \perp z$, where $\boldsymbol{x} = \boldsymbol{a}, \boldsymbol{y} = \boldsymbol{a} + 2\boldsymbol{b}, \boldsymbol{z} = \boldsymbol{c}$. (b) The in-plane electric polarization $\Delta P_{xy}(H)$ curves under $\theta = 45°$, where the θ is the angle between the z axis and H direction as shown in inset of (c). (c) The calculated results of θ dependence of ΔP_{xy}.

energy barrier between the ME-active state and ground ME-inactive state by over ∼meV. In other words, the strength of ME effect is highly dependent on the robustness of ground magnetic state. For example, the AFM order can sustain at very high T in type-I multiferroics, but the magnetic field is usually much difficult to drive considerable ME effect due to the strong AFM interaction (∼eV) [33]. In contrast, for many type-II multiferroics, such as the orthorhombic manganites $R\mathrm{MnO_3}$, the onset temperature of spiral order state is found rather low, because the strength of nearest-neighbor and further-neighbor magnetic exchanges usually have small values. In this case, spin order is very flexible to the magnetic field with comparable strength of energy barrier ∼meV, and ME effect is strong. Here, the magnetic susceptibility of $\mathrm{Co_2Mo_3O_8}$ shows stronger AFM interaction and no magnetic transition taking place in the xy plane. Hence, the external field is hard to modulate the magnetic structure, giving rise to weaker quadratic ME effect in the xy plane than that in the z direction ($\beta_{xxz} < \beta_{zzz}$). All of these results are consistent with the prediction of ME tensor with the magnetic point group $6'mm'$ in the AFM ground state.

It is natural to mention that the exchange-striction mechanism in the AFM state should contribute to the polarization and nonlinear ME effect, which is carefully reported in Ref. [24] for $\mathrm{Co_2Mo_3O_8}$, resembling the cases of $\mathrm{Fe_2Mo_3O_8}$ [19,22] and $\mathrm{Mn_2Mo_3O_8}$ [23] in the ground state. Upon the system entering into spin-flop transitions, the inverse Dzyaloshinskii-Moriya (IDM) mechanism should also be taken into consideration due to the noncollinear magnetic structures as shown Figs. 3(e) and 3(f). In this case, the high magnetic field prompts the competition between different exchange interactions, which drive the polarization switching through exchange-striction mechanism and IDM mechanism. In general, $\mathrm{Co_2Mo_3O_8}$ displays two consecutive SF transitions and polarization switching under high H, and is different from other linear ME materials in this 238 family.

IV. CONCLUSION

In summary, we have studied the metamagnetic transition and ME coupling effect under high magnetic field up to 60 T in $\mathrm{Co_2Mo_3O_8}$ single crystals. Two successive spin-flop transitions accompanied by colossal change of electric polarization are clearly observed. Furthermore, compared to its isostructural compounds, $\mathrm{Co_2Mo_3O_8}$ exhibits spin-flop transition and linear ME effect till H exceeding ∼27 T, thereby demonstrating a unique case in this 238 family. Our results are well consistent with the prediction of ME tensors, which provides a better approach to understand the evolution of magnetic structures and ME mechanism under high magnetic field.

ACKNOWLEDGMENT

This work was financially supported by the National Natural Science Foundation of China (Grants No. 11874031, No. 11834002, No. 92163210, No. 11774106, No. 11947092, No. 51721001, and No. 11974167).

[1] T. Kimura, T. Goto, H. Shintani, K. Ishizaka, T. Arima, and Y. Tokura, Magnetic control ferroelectric polarization, Nature (London) **426**, 55 (2003).

[2] S.-W. Cheong and M. Mostovoy, Multiferroics: A magnetic twist for ferroelectricity, Nat. Mater. **6**, 13 (2007).

[3] N. A. Spaldin and R. Ramesh, Advances in magnetoelectric multiferroics, Nat. Mater. **18**, 203 (2019).

[4] D. Khomskii, Classifying multiferroics: Mechanisms and effects, Physics **2**, 20 (2009).

[5] Y. Tokura, S. Seki, and N. Nagaosa, Multiferroics of spin origin, Rep. Prog. Phys. **77**, 076501 (2014).

[6] Y. J. Choi, H. T. Yi, S. Lee, Q. Huang, V. Kiryukhin, and S.-W. Cheong, Ferroelectricity in an Ising Chain Magnet, Phys. Rev. Lett. **100**, 047601 (2008).

[7] T. Kimura, G. Lawes, and A. P. Ramirez, Electric Polarization Rotation in a Hexaferrite with Long-Wavelength Magnetic Structures, Phys. Rev. Lett. **94**, 137201 (2005).

[8] Y. Kitagawa, Y. Hiraoka, T. Honda, T. Ishikura, H. Nakamura, and T. Kimura, Low-field magnetoelectric effect at room temperature, Nat. Mater. **9**, 797 (2010).

[9] C. L. Lu, M. H. Wu, L. Lin, and J.-M. Liu, Single-phase multiferroics: New materials, phenomena, and physics, Nat. Sci. Rev. **6**, 653 (2019).

[10] J. Wang, J. B. Neaton, H. Zheng, V. Nagarajan, S. B. Ogale, B. Liu, D. Viehland, V. Vaithyanathan, D. G. Schlom, U. V. Waghmare, N. A. Spldin, K. M. Rabe, M. Wuttig, and R. Ramesh, Epitaxial $BiFeO_3$ multiferroic thin film heterostructures, Science **299**, 1719 (2003).

[11] B. V. Aken, T. M. Palstra, A. Filippetti, and N. Spaldin, The origin of ferroelectricity in magnetoelectric $YMnO_3$, Nat. Mater. **3**, 164 (2004).

[12] L. Weymann, L. Bergen, T. Kain, A. Pimenov, A. Shuvaev, E. Constable, D. Szaller, B. V. Mill, A. M. Kuzmenko, V. Y. Ivanov, N. V. Kostyuchenko, A. I. Popov, A. K. Zvezdin, A. Pimenov, A. A. Mukhin, and M. Mostovoy, Unusual magnetoelectric effect in paramagnetic rare-earth langsite, npj Quantum. Mater. **5**, 61 (2020).

[13] S. M. Disseler, X. Luo, B. Gao, Y. S. Oh, R. W. Hu, Y. Z. Wang, D. Quintana, A. Zhang, Q. Huang, J. Lau, R. Paul, J. W. Lynn, S.-W. Cheong, and W. Ratcliff, Multiferroicity in doped hexagonal $LuFeO_3$, Phys. Rev. B **92**, 054435 (2015).

[14] A. Iyama and T. Kimura, Magnetoelelctric hysteresis loops in Cr_2O_3 at room temperature, Phys. Rev. B **87**, 180408(R) (2013).

[15] J. Zhang, N. Su, X. R. Mi, M. C. Pi, H. D. Zhou, J. G. Cheng, and Y. S. Chai, Probing magnetic symmetry in antiferromagnetic $Fe_4Nb_2O_9$ single crystal by linear magnetoelectric tensor, Phys. Rev. B **103**, L140401 (2021).

[16] S. H. Zheng, G. Z. Zhou, X. Li, M. F. Liu, Y. S. Tang, Y. L. Xie, M. Zeng, L. Lin, Z. B. Yan, X. K. Huang, X. P. Jiang, and J.-M. Liu, Remarkable magnetoelectric effect in single crystals of honeycomb magnet $Mn_4Nb_2O_9$, Appl. Phys. Lett. **117**, 072903 (2020).

[17] S.-W. Cheong, SOS: Symmetry-operational similarity, npj Quantum Mater. **4**, 53 (2019).

[18] S.-W. Cheong, Trompe l'oeil ferromagnetism, npj Quantum Mater. **5**, 37 (2020).

[19] T. Kurumaji, S. Ishiwata, and Y. Tokura, Doping-Tunable Ferrimagnetic Phase with Large Linear Magnetoelectric Effect in a Polar Magnet $Fe_2Mo_3O_8$, Phys. Rev. X **5**, 031034 (2015).

[20] J. W. Kim, S. Artyukhin, E. D. Mun, M. Jaime, N. Harrison, A. Hansen, J. J. Yang, Y. S. Oh, D. Vanderbilt, V. S. Zapf, and S.-W. Cheong, Succession Magnetic Field-Induced Transition and Colossal Magnetoelectric Effect in Ni_3TeO_6, Phys. Rev. Lett. **115**, 137201 (2015).

[21] Y. S. Tang, J. H. Zhang, L. Lin, R. Chen, J. F. Wang, S. H. Zheng, C. Li, Y. Y. Zhang, G. Z. Zhou, L. Huang, Z. B. Yan, X. M. Lu, D. Wu, X. K. Huang, X. P. Jiang, and J.-M. Liu, Metamagnetic transitions and magnetoelectricity in the spin-1 honeycomb antiferromagnet $Ni_2Mo_3O_8$, Phys. Rev. B **103**, 014112 (2021).

[22] Y. Z. Wang, G. L. Pascut, B. Gao, T. A. Tyson, K. Haule, V. Kiryukhin, and S.-W. Cheong, Unveiling hidden ferromagnetism and giant magnetoelectricity in polar magnet $Fe_2Mo_3O_8$, Sci. Rep. **5**, 12268 (2015).

[23] T. Kurumaji, S. Ishiwata, and Y. Tokura, Diagonal magnetoelectric susceptibility and effect of Fe doping in the polar ferrimagnet $Mn_2Mo_3O_8$, Phys. Rev. B **95**, 045142 (2017).

[24] Y. S. Tang, S. M. Wang, L. Lin, C. Li, S. H. Zheng, C. F. Li, J. H. Zhang, Z. B. Yan, X. P. Jiang, and J.-M. Liu, Collinear magnetic structure and multiferroicity in the polar magnet $Co_2Mo_3O_8$, Phys. Rev. B **100**, 134112 (2019).

[25] J. R. Morey, A. Scheie, J. P. Sheckelton, C. M. Brown, and T. M. McQueen, $Ni_2Mo_3O_8$: Complex antiferromagnetic order on a honeycomb lattice, Phys. Rev. Mater. **3**, 014410 (2019).

[26] S. P. McAlister and P. Strobel, Magnetic order in $M_2Mo_3O_8$ single crystals (M = Mn, Fe, Co, Ni), J. Magn. Magn. **30**, 340 (1983).

[27] H. Shiba, Y. Ueda, K. Okunishi, S. Kimura, and K. Kindo, Exchange interaction via crystal-field excited state and its importance in $CsCoCl_3$, J. Phys. Soc. Jpn. **72**, 2326 (2003).

[28] R. Chen, J. F. Wang, Z. W. Ouyang, Z. Z. He, S. M. Wang, L. Lin, J. M. Liu, C. L. Lu, Y. Liu, C. Dong, C. B. Liu, Z. C. Xia, A. Matsuo, Y. Kohama, and K. Kindo, Magnetic field induced ferroelectricity and half magnetization plateau in polycrystalline $R_2V_2O_7$ (R = Ni, Co), Phys. Rev. B **98**, 184404 (2018).

[29] J. F. Wang, M. Tokunaga, Z. Z. He, J. I. Yamaura, A. Matsuo, and K. Kindo, High magnetic field induced phases and half-magnetization plateau in the $S = 1$ kagome compound $Ni_3V_2O_8$, Phys. Rev. B **84**, 220407(R) (2011).

[30] K. J. Yoo, B. Koteswararao, J. H. Kang, A. Shahee, W. Y. Nam, F. F. Balakirev, V. S. Zapf, N. Harrison, A. Guda, N. T. Oganessian, and K. H. Kim, Magnetic field-induced ferroelectricity in $S = 1/2$ Kagome staircase compound $PbCu_3TeO_7$, npj Quantum Mater. **3**, 45 (2018).

[31] R. E. Newnham, *Properties of Materials: Anisotropy, Symmetry, Structure* (Oxford University Press, Oxford, 2005).

[32] J.-P. Rivera, On definitions, units, measurements, tensor forms of the linear magnetoelectric effect and on a new dynamic method applied to Cr-Cl boracite, Ferroelectrics **161**, 165 (1994).

[33] H. Das, A. L. Wysocki, Y. Geng, W. Wu, and C. J. Fennie, Bulk magnetoelectricity in the hexagonal manganites and ferrites, Nat. Commun. **5**, 2998 (2014).